

## Coordination Chemistry | Hot Paper |

## Altering Charges on Heterobimetallic Transition-Metal Carbonyl Clusters

Wiebke Unkrig, Konstantin Kloiber, Burkhard Butschke, Daniel Kratzert, and Ingo Krossing\*<sup>[a]</sup>

**Abstract:** The homoleptic group 5 carbonylates  $[\text{M}(\text{CO})_6]^-$  ( $\text{M} = \text{Nb}, \text{Ta}$ ) serve as ligands in carbonyl-terminated heterobimetallic  $\text{Ag}_m\text{M}_n$  clusters containing 3 to 11 metal atoms. Based on our serendipitous  $[\text{Ag}_6\{\text{Nb}(\text{CO})_6\}_4]^{2+}$  ( $4\mathbf{a}^{2+}$ ) precedent, we established access to such  $\text{Ag}_m\text{M}_n$  clusters of the composition  $[\text{Ag}_m\{\text{M}(\text{CO})_6\}_n]^x$  ( $\text{M} = \text{Nb}, \text{Ta}$ ;  $m = 1, 2, 6$ ;  $n = 2, 3, 4, 5$ ;  $x = 1-, 1+, 2+$ ). Salts of those molecular cluster ions were synthesized by the reaction of  $[\text{NEt}_4][\text{M}(\text{CO})_6]$  and  $\text{Ag}[\text{A}(\text{OR}^f)_4]$  ( $\text{R}^f = \text{C}(\text{CF}_3)_3$ ) in the correct stoichiometry in 1,2,3,4-tetrafluorobenzene at  $-35^\circ\text{C}$ . The solid-state structures were determined by single-crystal X-ray diffraction methods and,

owing to the thermal instability of the clusters, a limited scope of spectroscopic methods. In addition, DFT-based AIM calculations were performed to provide an understanding of the bonding within these clusters. Apparently, the clusters  $3^+$  ( $m=6, n=5$ ) and  $4^{2+}$  ( $m=6, n=4$ ) are superatom complexes with trigonal-prismatic or octahedral  $\text{Ag}_6$  superatom cores. The  $[\text{M}(\text{CO})_6]^-$  ions then bind through three CO units as tridentate chelate ligands to the superatom core, giving overall structures related to tetrahedral  $\text{AX}_4$  ( $4^{2+}$ ) or trigonal bipyramidal  $\text{AX}_5$  molecules ( $3^+$ ).

## Introduction

With the discovery of  $\text{Ni}(\text{CO})_4$ <sup>[1]</sup> the first homoleptic transition-metal carbonyl complex, a whole family of diversified complexes was born. This still growing family does not only include mononuclear,<sup>[2]</sup> but also bi-<sup>[3]</sup> and polynuclear<sup>[4,5]</sup> complexes with terminal, bridging, and even capping CO ligands. Owing to the synergistic bonding between the CO ligand and the metal atom, the carbonylates<sup>[2,6]</sup> and the neutral complexes<sup>[7]</sup> are the most stable and the most studied compounds of this group, whereas cationic<sup>[8,9]</sup> homoleptic carbonyl complexes are much more reactive. One reason for the continuing intensive interest in these complexes is certainly their wide range of applications in catalysis,<sup>[8]</sup> biochemical processes,<sup>[10]</sup> and medicine.<sup>[11]</sup>

In coordination chemistry, carbonyl complexes can also act as ligands for main-group or transition metals, thus forming heterometallic clusters. Carbonylates are used frequently to donate electrons to a main-group<sup>[12–16]</sup> or transition-metal<sup>[17]</sup> acceptor, whereas the capacity of neutral carbonyl complexes to

serve as electron donors is less pronounced. However, there are a few examples that contain neutral carbonyl complexes as donor ligands to main-group<sup>[12,18]</sup> or transition metals,<sup>[19–21]</sup> such as  $[(\text{OC})_5\text{Fe} \rightarrow \text{GaCl}_3]^{[22]}$  as well as  $[\text{Ag}\{\text{Fe}(\text{CO})_5\}_2]^+$ .<sup>[19,23]</sup> Overall, the heterometallic transition-metal carbonyl complexes are dominated by anionic clusters, with just a few neutral examples such as  $[\text{Ag}_4\{\text{Co}(\text{CO})_4\}_4]^{[24]}$ . To the best of our knowledge,  $[\text{Ag}\{\text{Fe}(\text{CO})_5\}_2]^+$ <sup>[19,23]</sup> is the only, albeit rather small, cationic and structurally characterized heterobimetallic homoleptic transition-metal carbonyl cluster so far.

In many of the larger transition-metal carbonyl cluster anions, a  $\text{M}_6$  octahedral core is the central structural motif. Figure 1 shows a selection of small carbonyl cluster anions containing an octahedral core, in which every second triangular surface is capped, thus creating a super-tetrahedron. The highly symmetric monometallic  $[\text{Os}_{20}(\text{CO})_{40}]^{2-}$ <sup>[5,25]</sup> (Figure 1a) even shows one more layer forming a “super-super-tetrahedron”. The structural motif shown in Figure 1b mainly appears in heterobimetallic cluster salts. Note that the ratio and posi-

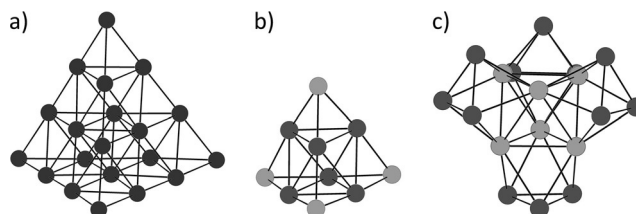


**Figure 1.** Metallic core of transition-metal clusters containing an octahedron, which is capped on every second triangular surface. The shown examples are the simplified crystal structures of (a)  $[\text{Os}_{20}(\text{CO})_{40}]^{2-}$ ,<sup>[5]</sup> (b)  $[\text{Cu}_6\{\text{Fe}(\text{CO})_4\}_4]^{2-}$ ,<sup>[17]</sup> (c)  $[\text{Au}_6\{\text{Ni}_3(\text{CO})_6\}_4]^{2-}$ .<sup>[27,28]</sup> The counterions and CO ligands were omitted for clarity.

[a] W. Unkrig, K. Kloiber, Dr. B. Butschke, Dr. D. Kratzert, Prof. Dr. I. Krossing  
Institut für Anorganische und Analytische Chemie  
Albert-Ludwigs-Universität Freiburg  
Albertstrasse 21, 79104 Freiburg (Germany)  
E-mail: krossing@uni-freiburg.de

Supporting information and the ORCID identification number(s) for the author(s) of this article can be found under:  
<https://doi.org/10.1002/chem.202002339>.

© 2020 The Authors. Published by Wiley-VCH GmbH. This is an open access article under the terms of Creative Commons Attribution NonCommercial License, which permits use, distribution and reproduction in any medium, provided the original work is properly cited and is not used for commercial purposes.

tions of the transition metals vary in the published complexes.<sup>[17,26]</sup>

The highly symmetric  $[\text{Au}_6\{\text{Ni}_3(\text{CO})_6\}_4]^{2-}$ <sup>[27,28]</sup> also belongs to this group (Figure 1 c). Three Ni atoms cap every other triangular face of the octahedral  $\text{Au}_6$  core, building a super-tetrahedron with  $T_d$  symmetry. Thus, the  $[\text{Ni}_3(\text{CO})_6]$  unit can be seen as a tridentate pseudo-ligand towards an  $\text{Au}_6$  superatom. Yet, it is challenging to fully understand the structural and bonding properties of such clusters. The superatom model<sup>[29]</sup> is one concept used to address these questions for molecular clusters. Thus, the calculated molecular orbitals of the cluster  $[\text{Au}_6\{\text{Ni}_3(\text{CO})_6\}_4]^{2-}$  are isolobal with those of the simple molecule  $\text{CH}_4$ . Therefore, the concept of hybridization was extended and the  $\text{Au}_6$  cluster orbitals were classified as  $sp^3$  hybrid orbitals.<sup>[28]</sup> By removing one, two, or three (pseudo-)ligands, analogies to  $\text{NH}_3$ ,  $\text{H}_2\text{O}$ , and  $\text{HCl}$  are obtained. However, the question remains as to what extent the concept can be transferred from metal-based pseudo-ligands to other systems. Sticking to this bonding concept, in principle, hitherto unknown coordination numbers of the  $\text{M}_6$  core exceeding four could be achieved, that is, five corresponding to a trigonal bipyramidal  $\text{AX}_5$  molecule.

Turning to known heterobimetallic carbonyl clusters with a silver core, the subject of this contribution, the large majority of structurally characterized examples contain the water-stable  $[\text{Fe}(\text{CO})_4]^{2-}$  ligand as a building block. The metallic core of all the known (anionic) structures with 3 to 13 silver atoms and with exterior  $[\text{Fe}(\text{CO})_4]$  units are collected in Figure 2.

Further examples of silver clusters with transition-metal carbonylates other than  $[\text{Fe}(\text{CO})_4]^{2-}$  are  $[\text{Ag}_9\text{Os}_{13}(\text{CO})_{48}]^-$ ,<sup>[33]</sup>  $[\text{Ag}_{16}\text{Ni}_{24}(\text{CO})_{40}]^{4-}$ ,<sup>[34]</sup> and  $[\text{Ag}_4\{\text{Co}(\text{CO})_4\}_4]$ .<sup>[24]</sup> In addition to the discussed heterobimetallic homoleptic carbonyl clusters, several related heteroleptic carbonyl complexes are known. For example, the first heterobimetallic carbonyl complexes, published by Nyholm and co-workers,<sup>[35]</sup> contained phosphine or cyclopentadienyl ligands. Yet, here, we focus on homoleptic clusters only including CO ligands.

In this publication, we present crystal structures and spectroscopic as well as bonding analyses of several heterobimetallic  $\text{Ag}_m\text{M}_n$  clusters ( $\text{M}=\text{Nb}, \text{Ta}$ ) containing 3 to 11 metal atoms. They obey the general formula  $[\text{Ag}_m\{\text{M}(\text{CO})_6\}_n]^x$  ( $\text{M}=\text{Nb}, \text{Ta}$ ,  $m=1, 2, 6$ ;  $n=2, 3, 4, 5$ ;  $x=1-, 1+, 2+$ ). Of those, only the structure of the super-tetrahedral cluster cation  $[\text{Ag}_6\{\text{Nb}(\text{CO})_6\}_4]^{2+}$  was communicated recently.<sup>[36]</sup> In these complexes, niobium or tantalum hexacarbonylates serve as ligands

for the silver atoms. For group 5 elements, structurally characterized heterometallic clusters are yet limited to only a few heteroleptic complexes. The neutral trimer  $[\text{AgM}(\text{CO})_4(\text{dmpe})]_3$  ( $\text{dmpe}=1,2\text{-bis}(\text{dimethylphosphino})\text{ethane}$ ,  $\text{M}=\text{Nb}, \text{Ta}$ )<sup>[37]</sup> appears to be the closest literature reference to the compounds in this work.

## Results and Discussion

During our continuing efforts to prepare novel transition-metal carbonyl cations<sup>[19,38]</sup> as salts of suitable and very weakly coordinating anions (WCAs),<sup>[39]</sup> we determined the crystal structure of  $[\text{Ag}_6\{\text{M}(\text{CO})_6\}_4]^{2+}([\text{Al}(\text{OR}^f)_4]^-)_2$  (**4a**;  $\text{R}^f=\text{C}(\text{CF}_3)_3$ ) by serendipity. The structure of the cluster cation adheres to Figure 1 b. It is an isolable intermediate towards the preparation of the heptacarbonyl salt  $[\text{Nb}(\text{CO})_7]^+[\text{Al}(\text{OR}^f)_4]^-$ .<sup>[36]</sup> The efforts towards the synthesis of further and related cluster salts are presented here.

### Syntheses and molecular structures of 1–4

With the intention to prepare homoleptic carbonyl cations, cluster salt **4a** was initially obtained from a reaction of  $[\text{NET}_4][\text{Nb}(\text{CO})_6]$  with  $\text{Ag}[\text{Al}(\text{OR}^f)_4]$  under 3 bar CO pressure.<sup>[36]</sup> Using this work as a starting point, we found that all syntheses to the heterobimetallic cluster ions described herein could be carried out in the absence of CO gas. This prevents the further reaction to homoleptic carbonyl cations as far as possible. With this route and using the polar, but non-coordinating solvent 4FB (1,2,3,4- $\text{F}_4\text{C}_6\text{H}_2$ ), a series of heterobimetallic cluster ions  $[\text{Ag}_m\{\text{M}(\text{CO})_6\}_n]^x$  ( $\text{M}=\text{Nb}, \text{Ta}$ ,  $m=1, 2, 6$ ;  $n=2, 3, 4, 5$ ;  $x=1-, 1+, 2+$ ) was synthesized. Their composition only represents the stoichiometric ratio used [Eq. (1)–(4); Scheme 1].

Neutral clusters like the hypothetical  $[\text{Ag}_3\{\text{M}(\text{CO})_6\}_3]$ —related to the trimer  $[\text{AgM}(\text{CO})_4(\text{dmpe})]_3$ <sup>[37]</sup>—were inaccessible. Rather decomposition was observed when using an equimolar ratio of the starting materials. All syntheses were carried out at  $-35^\circ\text{C}$ , close to the melting point of the solvent 4FB (m.p.  $-42^\circ\text{C}$ ). The intensely red salts were crystallized by storage at  $-30^\circ\text{C}$  after careful layering the reaction mixture with cold pentane at  $-30^\circ\text{C}$ . Powders were obtained at the same temperature by precipitation upon addition of cold pentane. Starting at about  $-15^\circ\text{C}$ , the compounds decomposed quickly with evolution of CO, leaving a brown solid, shown exemplary in Figure 3 for crystals of **4b**.

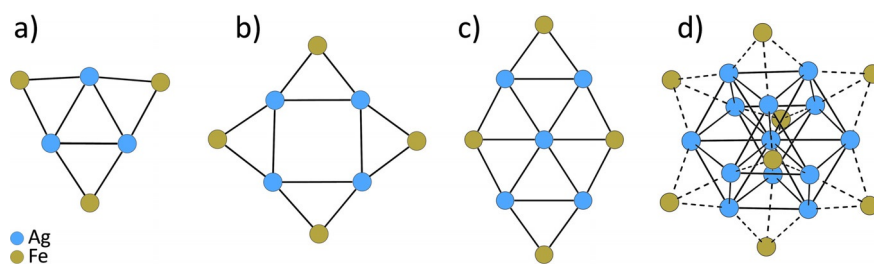
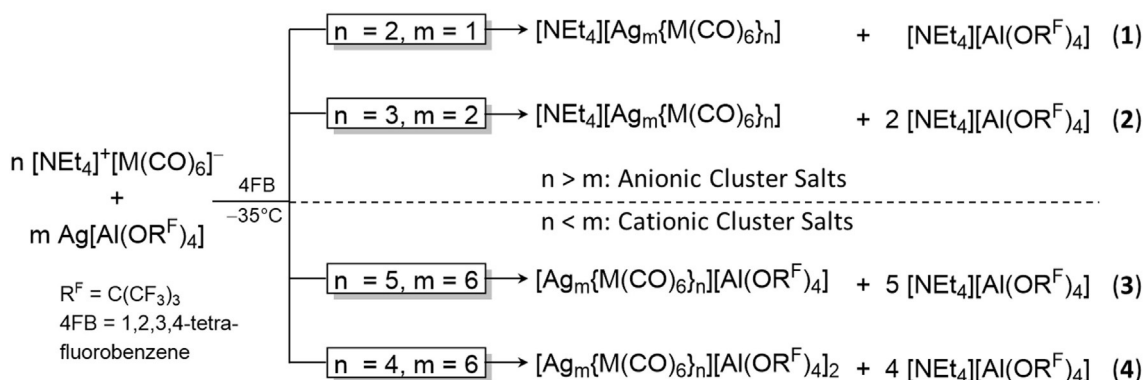


**Figure 2.** Metallic core arrangement of typical structurally characterized anionic homoleptic silver-iron carbonylate clusters. (a)  $[\text{Ag}_3\{\mu_2\text{-Fe}(\text{CO})_4\}_3]^{3-}$ <sup>[21]</sup>; (b)  $[\text{Ag}_4\{\mu_2\text{-Fe}(\text{CO})_4\}_4]^{4-}$ <sup>[21,30]</sup>; (c)  $[\text{Ag}_5\{\mu_2\text{-Fe}(\text{CO})_4\}_5]^{5-}$ <sup>[30]</sup>; (d)  $[\text{Ag}_{13}\{\text{Fe}(\text{CO})_6\}_4]^{14-}$ <sup>[31]</sup>,  $[\text{Ag}_{12}(\mu_{12}\text{-Ag})\{\mu_3\text{-Fe}(\text{CO})_4\}_6]^{5-}$ <sup>[32]</sup>



**Scheme 1.** Synthesis routes to  $[\text{NEt}_4][\text{Ag}\{\text{Nb}(\text{CO})_6\}_2]^-$  (**1a** M = Nb, **1b** M = Ta),  $[\text{NEt}_4][\text{Ag}_2\{\text{M}(\text{CO})_6\}_3]^-$  (**2a** M = Nb; **2b** M = Ta),  $[\text{Ag}_6\{\text{Nb}(\text{CO})_6\}_3]^+ [\text{Al}(\text{OR}^{\text{F}})_4]^-$  (**3a**), and  $[\text{Ag}_6\{\text{M}(\text{CO})_6\}_4]^{2+} [\text{Al}(\text{OR}^{\text{F}})_4]^{2-}$  (**4a** M = Nb; **4b** M = Ta).



**Figure 3.** Photographs of crystals of **4b** at  $-30^\circ\text{C}$  (left) and their quick decomposition at  $-15^\circ\text{C}$  with concomitant CO evolution (right).

### Molecular structures

Crystals suitable for single-crystal structure determinations of all compounds were obtained (Figure 5). For a better understanding, first the metallic cores of the cluster ions  $1^-$ ,  $2^-$ ,  $3^+$ , and  $4^{2+}$  including the schematic structural formulae of **1** to **4** are shown in Figure 4. Figure 5 then contains full ellipsoid plots of the carbonyl-terminated cluster ions. In all structures, both the  $[\text{NEt}_4]^+$  or the  $[\text{Al}(\text{OR}^{\text{F}})_4]^-$  counterions are well separated

and clearly non-coordinating, exhibiting their typical structural parameters. For brevity, they are not discussed.

Single-crystal X-ray structure determinations (scXRD) of mono-clinic **1a**, space group  $P2_1/c$ , revealed the formation of a  $C_2$ -symmetric anion  $1a^-$ . In the anion  $1a^-$ , two  $[\text{Nb}(\text{CO})_6]$  moieties coordinate one Ag atom almost linearly ( $\mu_1$ ; Nb–Ag–Nb  $174.03(1)^\circ$ ). Two almost equidistant Ag–Nb bonds at 2.8359(5) and 2.8467(5) Å are the key structural features (Figure 5). The closely related crystal structure of **1b** includes eight different pairs of ions in the asymmetric unit (Figure S16, Figure S17 in the Supporting Information), probably owing to the low Ag–Ta rotation barrier as previously described for the related cationic  $[\text{Ag}\{\text{Fe}(\text{CO})_5\}_2]^+$ .<sup>[19]</sup> Because of disorder and the large unit cell size, only X-ray data of inferior quality was acquired. Therefore, no structural parameters of this structure are discussed in the following. Nevertheless, the data clearly showed that the desired compound  $[\text{NEt}_4][\text{Ag}\{\text{Ta}(\text{CO})_6\}_2]$  was obtained.

Isomorphous **2a** and **2b** crystallized in the monoclinic space group  $C_2/c$  with the isostructural anions having almost  $C_2$  symmetry. Both structures contain two Ag atoms, each of which is linearly coordinated by two Nb or Ta atoms from  $[\text{M}(\text{CO})_6]$

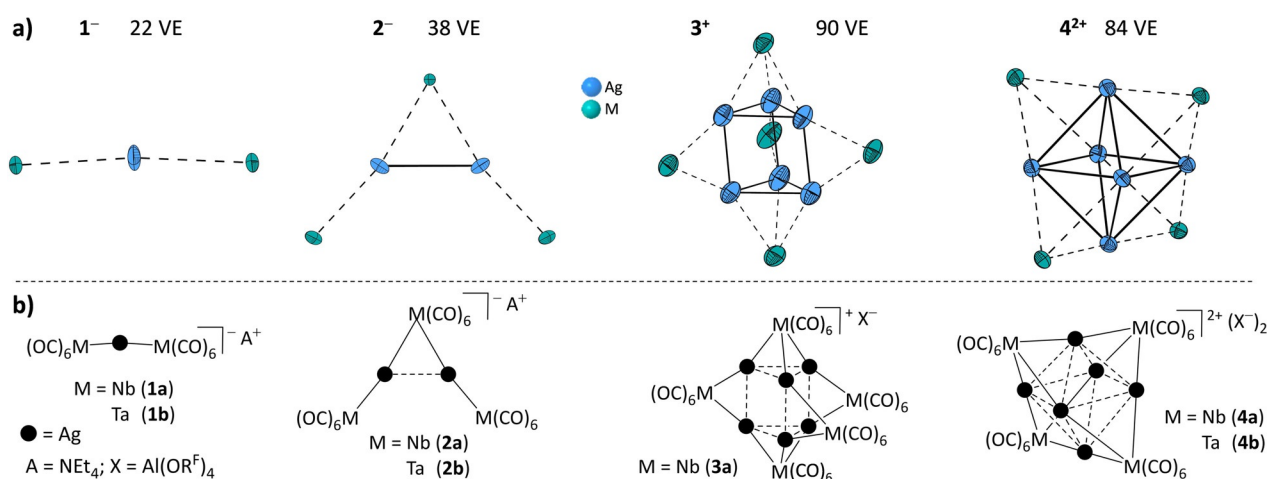


**Figure 4.** (a) Sum of the formally available valence electrons (VE) of the metal cores ( $\text{Ag}^+$ : 10 VE and  $\text{M}^-$ : 6 VE). Structures of the metallic cores of the anionic clusters  $1a^-$  (M = Nb) and  $1b^-$  (M = Ta),  $2a^-$  (M = Nb) and  $2b^-$  (M = Ta), as well as structures of the cationic cluster cores of  $3a^+$  (M = Nb),  $4a^{2+}$  (M = Nb), and  $4b^{2+}$  (M = Ta). The counterions  $[\text{NEt}_4]^+$  or  $[\text{Al}(\text{OR}^{\text{F}})_4]^-$  and the CO ligands are omitted for clarity in all structures. Ellipsoids were drawn at the 50% probability level. (b) Schematic structural formulae for **1**, **2**, **3**, and **4**.

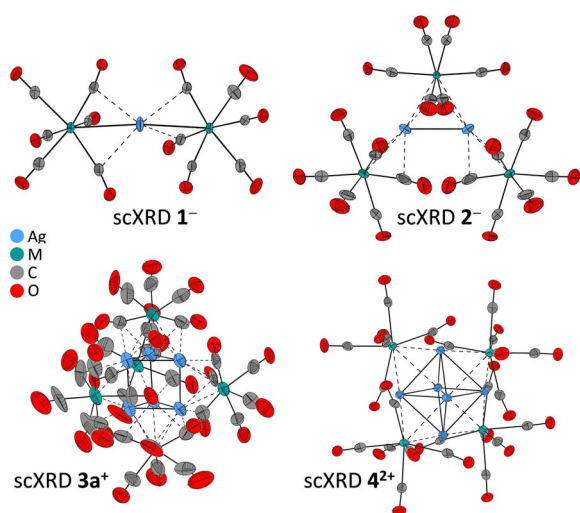


**Figure 5.** Molecular structures of the cluster ions within the single-crystal structures of 1–4 (anionic: **1a<sup>-</sup>** (M=Nb), **1b<sup>-</sup>** (M=Ta), **2a<sup>-</sup>** (M=Nb), and **2b<sup>-</sup>** (M=Ta); cationic **3a<sup>+</sup>** (M=Nb); dicationic **4a<sup>2+</sup>** (M=Nb) and **4b<sup>2+</sup>** (M=Ta). As the structures are almost identical for M=Nb and Ta, only one representation with M=Nb is shown. The counterions [NEt<sub>4</sub>]<sup>+</sup> or [Al(OR<sup>f</sup>)<sub>4</sub>]<sup>-</sup> were omitted for clarity. All thermal ellipsoids are drawn at the 50% probability level.

units. One apical [M(CO)<sub>6</sub>] unit is bound to two silver atoms (“μ<sub>2</sub>”), whereas the others interact only with one silver atom (“μ<sub>1</sub>”). The overall Ag<sub>2</sub>M<sub>3</sub> core is reminiscent of an “A-frame” structure (Figure 4).<sup>[40]</sup> The central Ag–Ag distance is equal to the metal–metal distances in metallic silver ( $d_{\text{Ag–Ag}}=2.889(1)$  Å (**2a<sup>-</sup>**),  $2.882(1)$  Å (**2b<sup>-</sup>**),  $d_{\text{Ag–metal}}=2.88$  Å).<sup>[41]</sup> In addition, the Ag–M distances ( $2.8081(8)$  to  $2.8710(7)$  Å) are in a similar range to the Ag–Ag separations. This suggests that **2a<sup>-</sup>** and **2b<sup>-</sup>** are delocalized formally 38 VE metal cluster anions.

Compound **3a** crystallized in the triclinic space group  $P\bar{1}$ . The structural core of **3a<sup>+</sup>** includes six Ag atoms arranged as a trigonal prism, which is capped by five [Nb(CO)<sub>6</sub>] fragments. Two are located on the triangular faces (“μ<sub>3</sub>”) whereas the other three are coordinating to the edges (“μ<sub>2</sub>”, Figure 4; Figure 5). Unfortunately, we could not get crystallographic data of sufficiently high quality for in depth discussion of light atom bond lengths and angles ( $R1=9.45\%$ ). Apparently, the CO ligands and also the heavy atoms are in motion, as visible from the size of the ellipsoids in the crystal structure (Figure 5). Yet, the metallic Nb<sub>5</sub>Ag<sub>6</sub> heavy atom core structure with formally 90 VE is well determined, exhibits almost  $D_{3h}$  symmetry and includes similar Ag–Ag (av.  $2.85$  Å) and Ag–Nb (av.  $2.96$  Å) distances. Both are close to the values in silver or niobium metal ( $d_{\text{Nb–metal}}=2.94$  Å). All attempts to obtain a similar structure with tantalum were futile.

Cluster salts **4a** and **4b** (Scheme 1) crystallized isomorphously in the orthorhombic space group  $Pbca$ . In the cluster dications **4a<sup>2+</sup>** and **4b<sup>2+</sup>**, four [M(CO)<sub>6</sub>] fragments cap a regular Ag<sub>6</sub> octahedron on every other triangular face (“μ<sub>3</sub>”; Figure 4; Figure 5). The structure cores of the dications are highly symmetric, adopt almost  $T_d$  symmetry, and form a hetero-bimetallic Ag<sub>6</sub>M<sub>4</sub> super-tetrahedron. Like in the other

compounds, the very similar Ag–Ag (av.  $2.90$  Å) and Ag–Nb (av.  $2.99$  Å) or Ag–Ta (av.  $2.98$  Å) distances are close to the values found in the pure metals (Ag:  $2.88$  Å; Nb and Ta:  $2.94$  Å). This observation suggests **4a<sup>2+</sup>** and **4b<sup>2+</sup>** to be delocalized formal 84 VE metal cluster dications. All bond lengths and angles given are summarized in Table S13 (in the Supporting Information).

Compared with the isolated octahedral anions [M(CO)<sub>6</sub>]<sup>-</sup>, the averaged M–C bond lengths of compounds 1 to 4 are elongated, and in accordance the respective C–O bond lengths are shortened with a higher Ag/M ratio leading to shorter CO bonds culminating in the dicationic structures **4<sup>2+</sup>** (Table 1, Table S14 in the Supporting Information). IR spectroscopic analysis in the next section supports this observation.

### Characterization by IR spectroscopy

Owing to the temperature sensitivity of the products, the IR spectroscopic analyses of the products **1**, **2**, **3**, and **4** were performed on the precipitated powders. Thus, the starting materials were dissolved in the correct ratio in cold 4FB in the glovebox and stirred at  $-35$  °C for 30 min. Then, the products were precipitated with cold pentane and were allowed to settle for another 30 min at  $-35$  °C. Afterwards, the solutions were decanted from the solid products and the remaining solvent was evaporated prior to the measurements on the precooled attenuated total reflection (ATR) unit of a FTIR spectrometer situated inside the glovebox. Figure 6a shows the ν(CO) range from experimental and calculated (BP86-D3(BJ)/def2-TZVPP) IR spectra of the starting material [NEt<sub>4</sub>][Nb(CO)<sub>6</sub>] and the cluster ions **1a<sup>-</sup>**, **2a<sup>-</sup>**, **3a<sup>+</sup>**, **4a<sup>2+</sup>**. In the adjacent graphic on the right (Figure 6b), the corresponding data with tantalum is shown. It must be noted that the calculated structures of **1<sup>-</sup>** include imaginary frequencies (**1a<sup>-</sup>**:  $-3.12$  cm<sup>-1</sup>, **1b<sup>-</sup>**:  $-15.07$  cm<sup>-1</sup>) which despite several attempts could not be relaxed. It appears that the potential energy surface is very flat and, despite tight conversion criteria, the converged structures are still slightly off the true minimum. However, this will not affect the vibrational and bonding analysis as indicated by the good agreement between optimized and experimental structures (cf. Table S3 to Table S6 in the Supporting Information). Furthermore, **1b<sup>-</sup>** converged only in the experimentally unrelated symmetry  $D_{3d}$ . This observation indicates a flat hypersurface and is consistent with the flexibility in the experimental crystal data of **1b<sup>-</sup>** discussed above (eight ion pairs in the asymmetric unit).

A precise assignment of the experimental bands was not possible, as the bands of the different clusters are quite broad and too similar to differentiate clearly. It is very likely that unreacted starting material was present in the samples of **1** and **2**, where the niobium/tantalum to silver ratio was quite high, resulting in very broad bands ranging between  $1920$ – $1530$  cm<sup>-1</sup>. In addition, it may be possible that different clusters exist in parallel and some of the precipitated samples could include mixtures. However, in agreement with single-crystal analysis, the patterns of the measured IR spectra confirm that stoichiometry influences at least the ratio of the re-

| Table 1. Experimental range of relevant bond lengths [Å] within the clustered ions of 1–4. <sup>[a]</sup> |         |                  |                  |                  |                                 |                   |                   |
|---|---------|------------------|------------------|------------------|---------------------------------|-------------------|-------------------|
| Bond  |         | 1 a <sup>-</sup> | 2 a <sup>-</sup> | 2 b <sup>-</sup> | 3 a <sup>+</sup> <sup>[b]</sup> | 4 a <sup>2+</sup> | 4 b <sup>2+</sup> |
| $d_{\text{Ag-M}}$   | $\mu_1$ | 2.836–2.847      | 2.808            | 2.817            | –                               | –                 | –                 |
|   | $\mu_2$ | –                | 2.867            | 2.871            | 2.891–2.952                     | –                 | –                 |
|   | $\mu_3$ | –                | –                | –                | 2.941–3.067                     | 2.966–3.015       | 2.966–3.016       |
| $d_{\text{Ag-C}}$   | $\mu_1$ | 2.544–2.669      | 2.505–2.629      | 2.524–2.597      | –                               | –                 | –                 |
|   | $\mu_2$ | –                | 2.551            | 2.568            | <i>2.57–2.70</i>                | –                 | –                 |
|   | $\mu_3$ | –                | –                | –                | <i>2.57–2.69</i>                | 2.592–2.701       | 2.582–2.706       |
| $d_{\text{M-C}}$  | $\mu_1$ | 2.111–2.150      | 2.107–2.149      | 2.091–2.128      | –                               | –                 | –                 |
|   | $\mu_2$ | –                | 2.124–2.164      | 2.110–2.141      | <i>2.07–2.21</i>                | –                 | –                 |
|   | $\mu_3$ | –                | –                | –                | <i>2.07–2.23</i>                | 2.110–2.219       | 2.102–2.173       |
| $d_{\text{CO,Ag}}$  | $\mu_1$ | 1.146–1.157      | 1.157–1.160      | 1.139–1.157      | –                               | –                 | –                 |
|   | $\mu_2$ | –                | 1.152            | 1.152            | <i>1.15–1.20</i>                | –                 | –                 |
|   | $\mu_3$ | –                | –                | –                | <i>1.13–1.21</i>                | 1.096–1.150       | 1.119–1.161       |
| $d_{\text{CO,free}}$  | $\mu_1$ | 1.137–1.140      | 1.133–1.164      | 1.124–1.150      | –                               | –                 | –                 |
|   | $\mu_2$ | –                | 1.126–1.149      | 1.131–1.151      | <i>1.10–1.24</i>                | –                 | –                 |
|   | $\mu_3$ | –                | –                | –                | <i>1.10–1.17</i>                | 1.098–1.166       | 1.113–1.153       |

[a] For comparison, the M–C bonds in  $[\text{M}(\text{CO})_6]^-$  are found on average at 2.089 [Nb<sup>[42]</sup>]/2.103 Å [Ta<sup>[43]</sup>] and the C–O bonds at 1.163 [Nb<sup>[42]</sup>]/1.149 Å [Ta<sup>[44]</sup>]. All structural parameters of the cluster ions are in very good agreement with the DFT calculated structures optimized at the BP86-D3(BJ)/def2-TZVPP level of theory. See the Supporting Information and Table S15 to Table S18 for a comparison. [b] Owing to poor quality of the crystallographic data, the values written in *italics* are only guidelines for reference purposes.

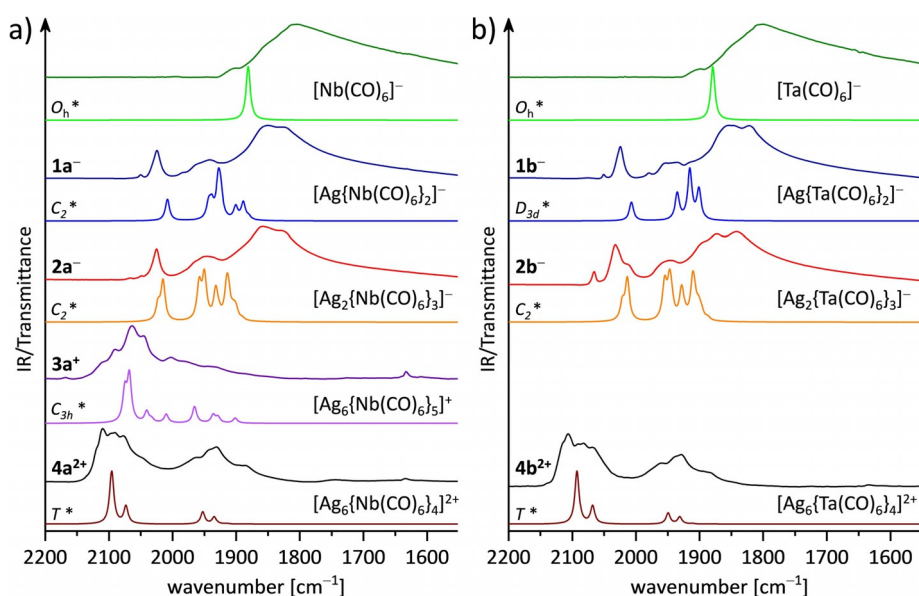


**Figure 6.** Section of the  $\nu_{\text{CO}}$  range from experimental and calculated IR spectra (\* BP86/D3(BJ)/def2-TZVPP). IR spectra of the starting materials  $[\text{NET}_x][\text{M}(\text{CO})_6]$  (top traces) and the precipitated powders with stoichiometries targeting at **1 a**, **2 a**, **3 a**, and **4 a** (a) or **1 b**, **2 b**, and **4 b** (b).

sulting molecules. Moreover, from the rather good qualitative agreement between experimental and calculated IR spectra, it appears very likely that at least for the cluster cations **3 a**<sup>+</sup>, **4 a**<sup>2+</sup>, and **4 b**<sup>2+</sup>, the majority of the material corresponds to the assigned clusters. Additionally, the experimental and calculated IR spectra demonstrate that the CO bands of the cationic clusters **3 a**<sup>+</sup>, **4 a**<sup>2+</sup>, and **4 b**<sup>2+</sup> are blueshifted compared with the CO bands in the anionic compounds **1**<sup>-</sup> and **2**<sup>-</sup> (Figure 6, Figure S1, Figure S2, Table S2 in the Supporting Information). This observation is in agreement with a reduced M–CO  $\pi$ -back

bonding character similar to the well examined bonding situation in homoleptic transition-metal carbonyl complexes.<sup>[45]</sup>

#### Atoms in molecules (AIM) analyses

A first formal rationalization of the cluster ions  $[\text{Ag}_m\{\text{M}(\text{CO})_6\}_n]^x$  yields their charges based on the interaction of the charged constituents:  $m\text{Ag}^+$  silver ions and  $n[\text{M}(\text{CO})_6]^-$  carbonylates yield the  $x=(m-n)$  cluster charge. To investigate how the charge is distributed within the  $[\text{M}(\text{CO})_6]$  moieties and the

silver cluster core and how the charges change upon complexation to silver, an atoms in molecules (AIM) analysis of the cluster ions  $1^-$  to  $4^{2+}$  was applied (Figure 7). For comparison, isolated  $[M(\text{CO})_6]^-$  was also assessed.

In addition, we performed natural bond orbital (NBO) analyses, but—as found previously<sup>[46]</sup>—this type of analysis trying to describe the bonding in the moiety in question as a set of electron precise natural Lewis structures, is not suitable to account for the heavily delocalized nature of the bonding in the clusters in question. Therefore, we concentrated here on the analysis of the topology of the electron density with AIM.

The charges of the integrated AIM metal atom basins within free  $[M(\text{CO})_6]^-$  (Nb +1.53; Ta +1.69) increase upon coordination to  $\text{Ag}^+$  only very slightly by +0.02 to +0.06. This holds regardless of the structure and total charge of the clusters (Table S7 in the Supporting Information). On the other hand, the positive charge residing on the silver atoms in each cluster

is rather low and is found to be in the range +0.11 ( $3\text{a}^+$ ) to +0.22 ( $1\text{a}^-$ ; Table S8 in the Supporting Information). This finding indicates that the entire  $[M(\text{CO})_6]$  fragment needs to be considered to deduce the bonding entities and their associated charge transfer relevant for the interaction with the silver core (Table S9 in the Supporting Information). Upon coordination, the charge residing on the  $[M(\text{CO})_6]$  fragments is reduced from  $-1$  in the free carbonylate down to at most +0.28/+0.31 in  $4^{2+}$ . This removal of electron density follows the M/Ag ratio: the lower this ratio, the higher is the positive charge on silver. Another trend is noticeable when the hapticity of the  $[M(\text{CO})_6]$  fragments is analyzed (Figure 7). The higher the hapticity, the higher is the net amount of electron transfer from the  $[M(\text{CO})_6]$  fragments to the silver atoms. As almost no change of the charges at Nb/Ta atoms was found upon complexation, the CO ligands have to contribute considerably (Table S10 in the Supporting Information). Within the free  $[M(\text{CO})_6]^-$  complexes, the  $\pi$ -back bonding is dominant and thereby delocalizes the anionic charge to a large extent towards the CO ligands, that is, the negative charge on those reaches  $-0.42$  (Nb) or  $-0.45$  (Ta). This transfer results in rather redshifted CO stretching frequencies ( $\nu_{\text{CO}}$ ) well below  $1900\text{ cm}^{-1}$ . Upon coordination to silver, these negative charges gradually decrease depending on the M/Ag ratio and go down to  $-0.11$  (Nb) or  $-0.12$  (Ta) in  $4^{2+}$ . Further, we note that the charges residing on the CO units differ for terminal ( $\text{CO}_{\text{terminal}}$ ) or additionally silver-bound ligands ( $\text{CO}_{\text{Ag}}$ ). The  $\text{CO}_{\text{Ag}}$  ligands deliver less electron density than the terminal ones and remain considerably more negatively charged at  $-0.33$  to  $-0.39$ . This observation suggests that the  $[M(\text{CO})_6]$  units coordinate via the  $\text{CO}_{\text{Ag}}$  moieties as chelating tridentate ligands to the silver atom(s). Apparently, cluster formation is strongly supported by the ligands. According to the AIM analysis, the negative charge transferred to the silver cores is delivered by the  $\text{CO}_{\text{terminal}}$  ligands (Figure 7).

This picture, based on the integrated charges of the AIM basins and included with Figure 7, is in full agreement with the calculated electron densities residing on the bond-critical points (bcps) of the clusters  $1^-$ ,  $2^-$ ,  $3^+$ , and  $4^{2+}$  and the parent ion  $[M(\text{CO})_6]^-$  (Table S12 in the Supporting Information). The isolated hexacarbonylate complexes  $[M(\text{CO})_6]^-$  show an electron density of  $0.62/0.65\text{ e}\text{\AA}^{-3}$  ( $M=\text{Nb}/\text{Ta}$ ) residing at the M–C critical points and  $3.09/3.08\text{ e}\text{\AA}^{-3}$  ( $M=\text{Nb}/\text{Ta}$ ) on the C–O bond paths (Figure S3 in the Supporting Information). In comparison, the charge density residing on these C–O bcps in the clusters increases with increasing positive charge and to a greater extent within the  $\text{CO}_{\text{terminal}}$  than within the  $\text{CO}_{\text{Ag}}$  ligands. This corresponds well to the experimental IR data, which indicate stronger CO bonds with increasing positive charge as seen by the blueshifted CO frequencies ( $\nu_{\text{CO}}$ ) described earlier and included with Figure 7. The electron densities on the M–C bond paths remain almost constant in all complexes. Turning to the cluster core, the electron density between the silver atoms decreases slightly with increasing number of clustered atoms. The electron density at the Ag–M and Ag–C bcps are comparable but typically higher for the Ag–C bond paths. The  $[M(\text{CO})_6]$  fragments thus appear to bind

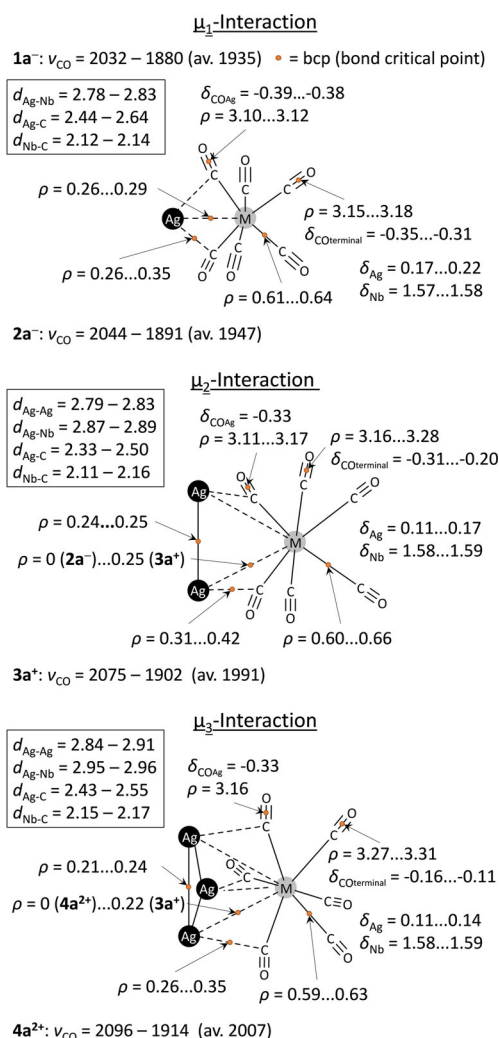


**Figure 7.** Schematic representations of the three  $\mu_1$ ,  $\mu_2$ , and  $\mu_3$ -bonding situations encountered within the cluster ions **1a–4a**. For clarity, only the niobium compounds were considered. AIM-calculated bond critical points (bcps), electron densities residing on bcps  $\rho$  [ $\text{e}\text{\AA}^{-3}$ ], partial charges on the metal atoms  $\delta_M$  or CO moieties  $\delta_{\text{CO}}$  [e], DFT-calculated bond lengths  $d$  [ $\text{\AA}$ ], and CO stretching frequencies  $\nu_{\text{CO}}$  [ $\text{cm}^{-1}$ ] are displayed.

more strongly to silver via the CO ligands than via the metal atom M. Interestingly, the standard parameters of the AIM analysis did not find Ag–M bcps for cluster  $4^{2+}$  (Figure S7 in the Supporting Information). In  $2^-$  (Figure S5 in the Supporting Information), only the M–Ag bond paths with the hapticity of one showed a clear bcp (Table S12 in the Supporting Information, marked with \*). This missing Ag–M interaction is apparently overcompensated by the coordination of the  $\text{CO}_{\text{Ag}}$  ligands, which seems to allow the formation of the cluster  $4^{2+}$  (Figure 8).

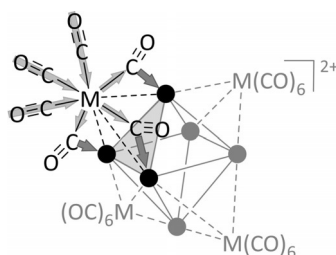


**Figure 8.** Schematic representation of the bonding situation in the cluster ion  $4^{2+}$ . The arrows indicate the shift of the electron density from the  $\text{CO}_{\text{terminal}}$  ligands through bridging  $\text{CO}_{\text{Ag}}$  ligands to the  $\text{Ag}_6$  cluster core. Note that in the AIM picture, a direct M–Ag interaction is absent as evidenced by the missing Ag–M bcp. Thus, the description as a super-tetrahedron as in Figure 1 b is only topological, but without bonding contribution.

Overall, it may be stated that the clusters form owing to electron transfer from the  $[\text{M}(\text{CO})_6]$  moieties to the silver core. The CO ligands play two major roles in the formation of these ions: 1) they serve as chelating anchors tethering the  $[\text{M}(\text{CO})_6]^-$  ligands to the silver core; 2) the  $\text{CO}_{\text{terminal}}$  ligands provide the electron density for the bonding within the larger trigonal prismatic or octahedral delocalized  $\text{Ag}_6$  cores. Roughly, five electrons are altogether transferred from the  $[\text{M}(\text{CO})_6]$  ligands to the  $\text{Ag}_6$  cores according to the AIM picture (Table S11 in the Supporting Information).

The interaction described in 2) apparently leads to the rather strong blueshift of the experimental CO stretching frequencies. In addition, the Ag–M interactions, if present at all, are rather weak. This observation is supported by the fact that—to our knowledge—binary silver–niobium and silver–tantalum alloys are unknown. Thus, the Ag–M interaction appears to be rather weak. Given the calculated charges at M ( $\approx +1.7$ ) and Ag ( $\approx +0.2$ ), such a bond would actually be expected to be much shorter than the observed distances of 2.81 to 3.07 Å (Table 1). Adding up the radii for  $\text{M}^{\text{III}}$  (0.72 Å; radius for  $\text{M}^{\text{II}}$  is unknown) and  $\text{Ag}^0$  (1.44 Å) gives approximately 2.16 Å as an approximation for a binding interaction. Altogether, this leads to the unexpected notion that the description of  $4^{2+}$  as a super-tetrahedron as shown in Figure 1 b is only topological, but without Ag–M bonding contribution. Thus, the central cluster unit in the large  $3^+$  and  $4^{2+}$  systems is the  $\text{Ag}_6$  core. This may be understood in terms of the superatom model, as presented in the next section.

### Structures $3^+$ and $4^{2+}$ in the context of the superatom model

Cluster ion  $4^{2+}$  may be compared with literature clusters, which were examined in more detail with regard to the superatom model. The octahedral  $\text{Ag}_6$  core of  $4^{2+}$ , which is capped by Nb/Ta atoms on every second triangular face forming the highly symmetric super-tetrahedron, has a structure related to the cluster  $[\text{Au}_6\text{X}_4]^{2+}$  ( $\text{X}=\text{F}, \text{Cl}, \text{Br}, \text{I}$ ) previously investigated with theoretical methods.<sup>[47]</sup> This cluster was considered as an analog of a tetrahedral molecule  $\text{CX}_4$  and  $\text{sp}^3$ -hybridization of the  $\text{Au}_6$  core was deduced. However, the earlier discussed AIM analysis of cluster  $4\text{a}^{2+}$  showed that in our case the CO ligands have the decisive role in the bonding rather than the Nb/Ta atoms. This reasoning allows for a comparison of compound  $4^{2+}$  with the cluster  $[\text{Au}_6\{\text{Ni}_3(\text{CO})_6\}_4]^{2-}$ <sup>[27,28]</sup> in Figure 9. The latter was also shown to be an analog of tetrahedral molecule  $\text{CH}_4$ .<sup>[28]</sup>

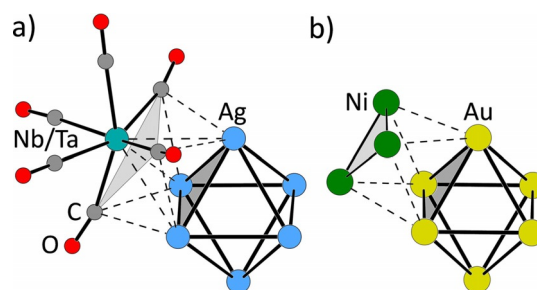


**Figure 9.** Schematic representations of a part of the structures of (a)  $[\text{Ag}_6\{\text{M}(\text{CO})_6\}_4]^{2+}$  ( $4^{2+}$ ) and (b)  $[\text{Au}_6\{\text{Ni}_3(\text{CO})_6\}_4]^{2-}$ .<sup>[27,28]</sup>

Every second face of the gold octahedron in Figure 9 b is capped by a  $[\text{Ni}_3(\text{CO})_6]$  unit. Using the published electron count of an  $[\text{Au}_6]^{2+}$  cluster core, this would include four  $[\text{Ni}_3(\text{CO})_6]^-$  radical anions as chelating pseudo-ligands. In  $4^{2+}$ , the chelating pseudo-ligand  $[\text{Ni}_3(\text{CO})_6]^-$  is exchanged for the tridentate  $\text{M}(\text{CO})_6^{\cdot}$  radical—iso-electronic to the known 17 valence electron metalloradical  $\text{V}(\text{CO})_6^{\cdot}$ —as a ligand to the  $\text{sp}^3$   $[\text{Ag}_6]^{2+}$  superatom.

By contrast, in structure  $3\text{a}^+$ , the prismatic  $\text{Ag}_6$  core is capped by five  $[\text{Nb}(\text{CO})_6]$  fragments, overall giving a  $D_{3h}$  trigonal bipyramid (Figure 10 b). The comparison with other clusters is quite difficult as only very few molecular clusters with this structural motif are known.<sup>[48]</sup> Nevertheless, according to the

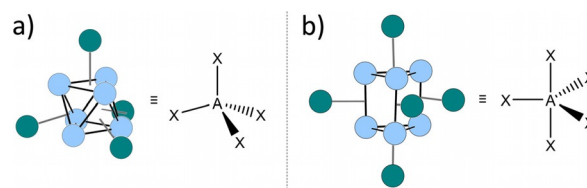


**Figure 10.** Schematic representations of the metal core of  $4^{2+}$  (a) and  $3^+$  rationalized by the superatom model as simple molecules generalized as  $\text{AX}_4$  (a) or  $\text{AX}_5$  (b).

lines rationalizing the super-tetrahedron in  $4^{2+}$  as  $sp^3$ , and being related to  $CH_4$  or generalized as  $AX_4$ ,<sup>[27,28]</sup> it is reasonable to argue that  $3a^+$  would correspond to trigonal bipyramidal  $SiH_5^-$ ,<sup>[49]</sup>  $NH_5$ ,<sup>[50]</sup>  $PH_5$ ,<sup>[51]</sup> or generalized to an  $AX_5$  molecule as shown in Figure 10.

However, to enable a firm classification of the cluster cores of compounds  $3^+$  and  $4^{2+}$  as superatoms, further intensive theoretical investigations are necessary and we would be very pleased if another research group with more experience in this field would take up this topic.

## Conclusion

Several heterobimetallic formal  $Ag_mM_n$  clusters ( $M=Nb, Ta$ ) with the general formula  $[Ag_m\{M(CO)_6\}_n]^x$  ( $M=Nb, Ta$ ;  $m=1, 2, 6$ ;  $n=2, 3, 4, 5$ ;  $x=1-, 1+, 2+$ ) were prepared, structurally and spectroscopically analyzed, and their bonding was investigated. As an addition to known anionic and neutral heterobimetallic  $Ag-M$  carbonyl clusters, we present the first examples including the  $[M(CO)_6]$  moiety as a component of anionic clusters. Furthermore, the first larger cationic clusters of this kind were obtained, stabilized by a weakly coordinating anion. They include a  $D_{3h}$ -symmetric  $Ag_6Nb_5$  or  $T_d$ -symmetric  $Ag_6M_4$  core ( $M=Nb, Ta$ ). The discussion of the crystal structures, IR data, and quantum calculations showed indications for a peculiar bonding situation in these clusters: The  $[M(CO)_6]$  groups can be seen as chelate ligands to the silver core. The CO ligands of the M carbonylates play a significant role, as they provide the electron density for the bonding and act as chelating anchors to the silver core. Thus, apparently the  $[M(CO)_6]$  units in  $3^+$  or  $4^{2+}$  serve as ligands to the  $Ag_6$  superatom. In  $4^{2+}$ , this follows the lines as described for  $[Au_6X_4]^{2+}$  ( $X=F, Cl, Br, I$ ),<sup>[47]</sup> which was considered as an  $AX_4$  analogue with  $sp^3$ -hybridization of the  $[Au_6]^{2+}$  core. The structure of  $3^+$  possibly is the first example of an extension to an  $AX_5$  analogue. The hybridization of the underlying trigonal prismatic  $Ag_6$  superatom would be interesting to be analyzed by groups with a particular focus on theoretical chemistry. Thus, we encourage other research groups to further investigate the clusters quantum chemically in terms of the superatom model or with other suitable approaches.

## Experimental Section

**Crystallographic data:** Deposition numbers 1998854, 1998851, 1998852, 1998853, 1909279, and 1998922 (**1a**, **2a**, **2b**, **3a**, **4a**, and **4b**) contain(s) the supplementary crystallographic data for this paper. These data are provided free of charge by the joint Cambridge Crystallographic Data Centre and Fachinformationszentrum Karlsruhe Access Structures service..

## Acknowledgments

Open access funding was enabled and organized by Projekt DEAL.

## Conflict of interest

The authors declare no conflict of interest.

**Keywords:** carbonyl clusters • charge • DFT • heterobimetallic compounds • silver

- [1] L. Mond, C. Langer, F. Quincke, *J. Chem. Soc. Trans.* **1890**, 57, 749.
- [2] J. M. Maher, R. P. Beatty, N. J. Cooper, *Organometallics* **1985**, 4, 1354.
- [3] L. B. Handy, J. K. Ruff, L. F. Dahl, *J. Am. Chem. Soc.* **1970**, 92, 7312.
- [4] a) P. F. Jackson, B. F. G. Johnson, J. Lewis, M. McPartlin, W. J. H. Nelson, *J. Chem. Soc. Chem. Commun.* **1979**, 735; b) B. F. G. Johnson, *Coord. Chem. Rev.* **1999**, 190–192, 1269.
- [5] L. H. Gade, B. F. G. Johnson, J. Lewis, M. McPartlin, H. R. Powell, P. R. Raithby, W.-T. Wong, *J. Chem. Soc. Dalton Trans.* **1994**, 521.
- [6] a) W. Beck, *Angew. Chem. Int. Ed. Engl.* **1991**, 30, 168; *Angew. Chem.* **1991**, 103, 173; b) J. E. Ellis, *Organometallics* **2003**, 22, 3322.
- [7] a) G. G. Sumner, H. P. Klug, L. E. Alexander, *Acta Crystallogr.* **1964**, 17, 732; b) A. W. Hanson, *Acta Crystallogr.* **1962**, 15, 930.
- [8] Q. Xu, *Coord. Chem. Rev.* **2002**, 231, 83.
- [9] a) H. Willner, F. Aubke, *Organometallics* **2003**, 22, 3612; b) H. Willner, F. Aubke, *Chem. Eur. J.* **2003**, 9, 1668; c) J. Geier, H. Willner, C. W. Lehmann, F. Aubke, *Inorg. Chem.* **2007**, 46, 7210; d) M. Finze, E. Bernhardt, H. Willner, C. W. Lehmann, F. Aubke, *Inorg. Chem.* **2005**, 44, 4206.
- [10] a) G. Jaouen, A. Vessieres, S. Top, A. A. Ismail, I. S. Butler, *J. Am. Chem. Soc.* **1985**, 107, 4778; b) A. Monney, M. Albrecht, *Coord. Chem. Rev.* **2013**, 257, 2420.
- [11] a) T. R. Johnson, B. E. Mann, J. E. Clark, R. Foresti, C. J. Green, R. Motterlini, *Angew. Chem. Int. Ed.* **2003**, 42, 3722; *Angew. Chem.* **2003**, 115, 3850; b) B. E. Mann, *Organometallics* **2012**, 31, 5728.
- [12] J. Bauer, H. Braunschweig, R. D. Dewhurst, *Chem. Rev.* **2012**, 112, 4329.
- [13] R. A. Fischer, A. Miehr, H. Hoffmann, W. Rogge, C. Boehme, G. Frenking, E. Herdtweck, *Z. Anorg. Allg. Chem.* **1999**, 625, 1466.
- [14] L. M. Clarkson, K. McCrudden, N. C. Norman, L. J. Farrugia, *Polyhedron* **1990**, 9, 2533.
- [15] E. Leiner, O. Hampe, M. Scheer, *Eur. J. Inorg. Chem.* **2002**, 584.
- [16] P. Rutsch, G. Renner, G. Huttner, S. Sandhöfner, *Z. Naturforsch. B* **2002**, 57, 757.
- [17] G. Doyle, K. A. Eriksen, D. van Engen, *J. Am. Chem. Soc.* **1985**, 107, 7914.
- [18] R. Bissert, H. Braunschweig, R. D. Dewhurst, C. Schneider, *Organometallics* **2016**, 35, 2567.
- [19] P. J. Malinowski, I. Krossing, *Angew. Chem. Int. Ed.* **2014**, 53, 13460; *Angew. Chem.* **2014**, 126, 13678.
- [20] V. G. Albano, F. Azzaroni, M. C. Iapalucci, G. Longoni, M. Monari, S. Mulley, *MRS Proc.* **1992**, 272, 115.
- [21] B. Berti, M. Bortoluzzi, C. Cesari, C. Femoni, M. C. Iapalucci, R. Mazzoni, F. Vacca, S. Zacchini, *Inorg. Chem.* **2019**, 58, 2911.
- [22] H. Braunschweig, R. D. Dewhurst, F. Hupp, C. Kaufmann, A. K. Phukan, C. Schneider, Q. Ye, *Chem. Sci.* **2014**, 5, 4099.
- [23] G. Wang, Y. S. Ceylan, T. R. Cundari, H. V. R. Dias, *J. Am. Chem. Soc.* **2017**, 139, 14292.
- [24] P. Klüfers, *Z. Kristallogr. Cryst. Mater.* **1984**, 166, 143.
- [25] P. J. Dyson, J. S. McIndoe, *Transition-Metal Carbonyl Cluster Chemistry*, CRC Press, Amsterdam, **2019**.
- [26] T. Chihara, M. Sato, H. Konomoto, S. Kamiguchi, H. Ogawa, Y. Wakatsuki, *J. Chem. Soc. Dalton Trans.* **2000**, 2295.
- [27] A. J. Whoolery, L. F. Dahl, *J. Am. Chem. Soc.* **1991**, 113, 6683.
- [28] A. Muñoz-Castro, *Chem. Sci.* **2014**, 5, 4749.
- [29] a) S. N. Khanna, P. Jena, *Phys. Rev. B Condens. Matter* **1995**, 51, 13705; b) S. N. Khanna, P. Jena, *Phys. Rev. Lett.* **1992**, 69, 1664; c) J. U. Reveles, S. N. Khanna, P. J. Roach, A. W. Castleman, *Proc. Natl. Acad. Sci. USA* **2006**, 103, 18405.
- [30] V. G. Albano, F. Azzaroni, M. C. Iapalucci, G. Longoni, M. Monari, S. Mulley, D. M. Proserpio, A. Sironi, *Inorg. Chem.* **1994**, 33, 5320.
- [31] V. G. Albano, L. Grossi, G. Longoni, M. Monari, S. Mulley, A. Sironi, *J. Am. Chem. Soc.* **1992**, 114, 5708.
- [32] D. Collini, C. Femoni, M. C. Iapalucci, G. Longoni, *C. R. Chim.* **2005**, 8, 1645.

- [33] Y.-B. Lee, W.-T. Wong, *Chem. Commun.* **2007**, 3924.
- [34] J. Zhang, L. F. Dahl, *J. Chem. Soc. Dalton Trans.* **2002**, 1269.
- [35] C. E. Coffey, J. Lewis, R. S. Nyholm, *J. Chem. Soc.* **1964**, 1741.
- [36] W. Unkrig, M. Schmitt, D. Kratzert, D. Himmel, I. Krossing, *Nat. Chem.* **2020**, *12*, 647.
- [37] F. Calderazzo, G. Pampaloni, U. Englert, J. Strähle, *Angew. Chem. Int. Ed. Engl.* **1989**, *28*, 471; *Angew. Chem.* **1989**, *101*, 469.
- [38] a) J. Schaefer, A. Kraft, S. Reiningger, G. Santiso-Quinones, D. Himmel, N. Trapp, U. Gellrich, B. Breit, I. Krossing, *Chem. Eur. J.* **2013**, *19*, 12468; b) S. C. Meier, D. Himmel, I. Krossing, *Chem. Eur. J.* **2018**, *24*, 19348; c) J. Bohnenberger, B. Derstine, M. Daub, I. Krossing, *Angew. Chem. Int. Ed.* **2019**, *58*, 9586; *Angew. Chem.* **2019**, *131*, 9687; d) J. Bohnenberger, I. Krossing, *Angew. Chem. Int. Ed.* **2020**, *59*, 5581; *Angew. Chem.* **2020**, *132*, 5629; e) J. Bohnenberger, M. Schmitt, W. Feuerstein, I. Krummenacher, B. Butschke, J. Czajka, P. J. Malinowski, F. Breher, I. Krossing, *Chem. Sci.* **2020**, *11*, 3592; f) S. C. Meier, A. Holz, A. Schmidt, D. Kratzert, D. Himmel, I. Krossing, *Chem. Eur. J.* **2017**, *23*, 14658; g) J. Bohnenberger, W. Feuerstein, D. Himmel, M. Daub, F. Breher, I. Krossing, *Nat. Commun.* **2019**, *10*, 624.
- [39] a) I. Krossing, *Chem. Eur. J.* **2001**, *7*, 490; b) I. M. Riddlestone, A. Kraft, J. Schaefer, I. Krossing, *Angew. Chem. Int. Ed.* **2018**, *57*, 13982; *Angew. Chem.* **2018**, *130*, 14178.
- [40] a) R. J. Puddephatt, *Chem. Soc. Rev.* **1983**, *12*, 99; b) C. P. Kubiak, R. Eisenberg, *J. Am. Chem. Soc.* **1977**, *99*, 6129; c) G. S. Ferguson, P. T. Wolczanski, L. Parkanyi, M. C. Zonneville, *Organometallics* **1988**, *7*, 1967; d) C. P. Kubiak, R. Eisenberg, *Inorg. Chem.* **1980**, *19*, 2726.
- [41] A. Bondi, *J. Phys. Chem.* **1964**, *68*, 441.
- [42] F. Calderazzo, G. Pampaloni, G. Pelizzi, *J. Organomet. Chem.* **1982**, *233*, C41.
- [43] F. A. Cotton, C. A. Murillo, X. Wang, *Inorganica Chim. Acta* **2000**, *300–302*, 1.
- [44] F. Calderazzo, U. Englert, G. Pampaloni, G. Pelizzi, R. Zamboni, *Inorg. Chem.* **1983**, *22*, 1865.
- [45] H. Willner, F. Aubke, *Angew. Chem. Int. Ed. Engl.* **1997**, *36*, 2402; *Angew. Chem.* **1997**, *109*, 2506.
- [46] I. M. Riddlestone, P. Weis, A. Martens, M. Schorpp, H. Scherer, I. Krossing, *Chem. Eur. J.* **2019**, *25*, 10546.
- [47] A. Muñoz-Castro, R. B. King, *Int. J. Quantum Chem.* **2017**, *117*, e25331.
- [48] a) J. C. Calabrese, L. F. Dahl, P. Chini, G. Longoni, S. Martinengo, *J. Am. Chem. Soc.* **1974**, *96*, 2614; b) Y.-T. Chen, I. S. Krytchankou, A. J. Karttunen, E. V. Grachova, S. P. Tunik, P.-T. Chou, I. O. Koshevoy, *Organometallics* **2017**, *36*, 480.
- [49] D. J. Hajdasz, Y. Ho, R. R. Squires, *J. Am. Chem. Soc.* **1994**, *116*, 10751.
- [50] G. A. Olah, D. J. Donovan, J. Shen, G. Klopman, *J. Am. Chem. Soc.* **1975**, *97*, 3559.
- [51] S.-K. Shih, S. D. Peyerimhoff, R. J. Buenker, *J. Chem. Soc. Faraday Trans. 2* **1979**, *75*, 379.

---

Manuscript received: May 12, 2020

Revised manuscript received: June 16, 2020

Accepted manuscript online: July 2, 2020

Version of record online: September 11, 2020